



HAL
open science

Scattering of neutral particles by a two-dimensional exponential corrugated potential

G. Armand

► **To cite this version:**

G. Armand. Scattering of neutral particles by a two-dimensional exponential corrugated potential. *Journal de Physique*, 1980, 41 (12), pp.1475-1486. 10.1051/jphys:0198000410120147500 . jpa-00208975

HAL Id: jpa-00208975

<https://hal.science/jpa-00208975>

Submitted on 4 Feb 2008

HAL is a multi-disciplinary open access archive for the deposit and dissemination of scientific research documents, whether they are published or not. The documents may come from teaching and research institutions in France or abroad, or from public or private research centers.

L'archive ouverte pluridisciplinaire **HAL**, est destinée au dépôt et à la diffusion de documents scientifiques de niveau recherche, publiés ou non, émanant des établissements d'enseignement et de recherche français ou étrangers, des laboratoires publics ou privés.

Classification

Physics Abstracts

03.80 — 61.14D — 68.20

Scattering of neutral particles by a two-dimensional exponential corrugated potential

G. Armand

Centre d'Etudes Nucléaires de Saclay, Service de Physique Atomique, Section d'Etudes des Interactions Gaz-Solides,
B.P. N° 2, 91190 Gif sur Yvette, France

(Reçu le 25 avril 1980, révisé le 12 août, accepté le 21 août 1980)

Résumé. — L'équation intégrale de la diffusion est résolue exactement dans le cas d'un potentiel exponentiel gaufré bidimensionnel. L'on obtient un ensemble infini d'équations intégrales couplées, contenant des fonctions inconnues proportionnelles aux amplitudes des ondes. Cet ensemble est traité numériquement en utilisant le processus itératif de Neumann. Pour une surface ayant une cellule carrée et un profil de corrugation sinusoidal, le domaine de convergence est déterminé. Les résultats numériques sont comparés à ceux obtenus en traitant la diffusion par un potentiel de mur dur gaufré.

La pente finie du potentiel exponentiel produit une augmentation de l'intensité du faisceau spéculaire et une réduction de toutes les autres intensités. Ce fait s'explique qualitativement en considérant la pénétration des ondes dans le potentiel.

Les singularités apparaissant dans les intensités des différents faisceaux lorsque l'un d'eux émerge sont analysées. Elles sont de deux types, et dépendent du couplage entre le faisceau considéré et le faisceau émergent. Leur forme et amplitude sont fortement dépendantes du coefficient d'amortissement de l'exponentielle et leur mesure devrait permettre la détermination de cette quantité.

Abstract. — The integral equation for the scattering is solved exactly for a two-dimensional exponential corrugated potential. An infinite set of coupled integral equations involving a function proportional to the wave amplitude has been found. This set is numerically solved by a Neumann iterative process. For a surface square unit cell and a sinusoidal corrugation profile, the convergence domain is determined and numerical results are obtained which are compared to those given by the hard corrugated wall potential.

The finite slope of the potential yields an enhancement of the specular intensity and a reduction of all the others. This is qualitatively explained by considering of wave penetration.

The singularities which appear in the different beam intensities when a beam is emerging are analysed. They are of two types depending on whether the beam is strongly coupled or not to the emerging one. As their shape and amplitude depend strongly upon the damping coefficient of the exponential, their measurement could allow the determination of this quantity.

1. **Introduction.** — Experimental data for the scattering of neutral particles by a periodic surface are in numerous cases compared to calculated intensities obtained with the hard corrugated wall potential (HCWP) defined by

$$V = \infty \quad z < \varphi(x, y)$$

$$V = 0 \quad z > \varphi(x, y) .$$

Generally one determines a periodic corrugation function φ which gives the best fit between experimental and calculated intensities (see for instance refs. [1, 2]). This function gives something like the electronic isodensity profile on the surface, the

periodicity of which coincides generally with the atomic surface periodicity. Therefore this function is often called surface profile.

Furthermore the HCWP with a well having a long-range attractive part varying as z^{-3} [3, 4], gives a good description of the structures observed experimentally in the diffracted beams in the vicinity of conditions for which resonance with bound states is satisfied.

On the other hand, from the observation of these resonances one deduces the energy of the bound states. In all cases a Morse, or a nine-three, or more elaborate potential of this type [5] gives good agreement between calculated energy levels and the experi-

mental data. This gives the zero order Fourier component of the potential which has in the repulsive region a finite slope.

In fact, the adjustment of the energy levels is not very sensitive to the stiffness of the repulsive potential part in the continuum region and hence the fit to beam intensities is probably a better way to determine this repulsive part.

At short distances from the surface the overlap of the electronic wave functions of the incident atom and the crystal surface is responsible for the appearance of repulsive forces. Usually this does not lead to a potential of infinite stiffness and this qualitative conclusion is confirmed by a reliable potential calculation [6]. Hence the HCWP is only an approximate representation of the real potential.

Thus the following question arises : why does the HCWP seem to be so successful in interpreting the experimental data ? In part the answer may lie in the quality of available data. In an experimental set up the incident beam is not strictly monoenergetic and has a small but finite angular spread, and the same is true for the detector. Consequently the diffracted peaks are broadened, the broadening being a function of incident angle and diffraction order. Also the crystal has a finite temperature yielding an attenuation of the measured intensities. Therefore it is necessary to correct for peak broadening and to measure the thermal attenuation of intensity in order to extrapolate to zero temperature if one wants to make a precise comparison with the calculated intensities. To the author's knowledge there is just one reported result where the two corrections have been made [2]. Even in this work, after correction, the experimental unitarity is less than 0.8 which is probably due to incoherent in plane or out of plane scattering. In these conditions an approximate potential such as the HCWP, could give a good representation of the experimental data.

With intensity measurements now becoming more and more precise, it seems necessary to work theoretically with a less approximate potential. It is then natural to consider a potential of finite stiffness which, contrary to HCWP, allows wave penetration. This effect has been modelled previously by using a HCWP of finite height ($V = V_0$, $z < \varphi(x, y)$) called the *soft wall potential* [7]. The results show a significant effect on the calculated beam intensities as the height V_0 decreases. Nevertheless this seems to be an improper way to represent physical reality. In order to have a more realistic picture we have considered recently [8] the one-dimensional exponential corrugated potential (ECP)

$$V = C \exp[-\chi(z - \varphi(x))]$$

which gives the HCWP as χ goes to infinity. The scattering problem has been solved without approximation. Numerical calculations imply the solution of an infinite set of coupled integral equations. With

the procedure adopted a convergent solution is obtained only with small corrugation amplitude. In the domain of convergence numerical results show clearly that, compared to a hardwall, a soft potential enhances the specular and reduces the intensity of all other diffracted beams. The wave penetration reduces the effect of multiple scattering.

In this paper the theoretical developments are presented with more details for a two-dimensional surface with corrugation function $\varphi(x, y)$. A set of coupled integral equations is obtained as before but here the unknown functions are the t matrix elements which are directly linked to the scattered wave amplitude. This set is solved by an iterative process. Compared to the previous work the domain of convergence is further extended. Particular numerical results are reported for the case when, varying the incident angle, a beam emerges from a closed to an open channel.

Similar previous works are the so-called coupled channel calculations initiated by Wolken [9] in which the infinite set of coupled differential equation is solved numerically. Generally the authors take account of only a few potential Fourier components. All these components are included in the ECP calculation and therefore the two potentials used in these two different approaches are substantially different.

2. General theory. — The starting point is the integral form of the Schrödinger equation in the two-potential formalism :

$$|\psi_i^+\rangle = |\phi_i\rangle + (E_i - H_0 + i\epsilon)^{-1} \times [V(\mathbf{R}, z) - U(z)] |\psi_i^+\rangle \quad (1)$$

with

$$H_0 = -\frac{\hbar^2}{2m} \nabla^2 + U(z).$$

As usual the direction Oz is taken normal to the surface, and respectively a position \mathbf{r} or a wave vector \mathbf{k} is decomposed into parallel (\mathbf{R}, \mathbf{K}) and normal (z, k_z) components to the surface.

The two potentials V and U are assumed to have only positive values and to be continuous decreasing functions of z . $U(z)$ is chosen in such a way that the continuous sets of eigenvalues e_p and eigenfunctions $e^{i\mathbf{K}\cdot\mathbf{R}} \phi_p(z)$ of H_0 are known.

Letting

$$\int_{-\infty}^{+\infty} \phi_q^*(z) \phi_p(z) dz = B^2 \delta(q - p) \quad (2)$$

the projection operator is given by

$$P = \frac{1}{4\pi^2 B^2} \int_{-\infty}^{+\infty} d\mathbf{K} |e^{i\mathbf{K}\cdot\mathbf{R}}\rangle \langle e^{i\mathbf{K}\cdot\mathbf{R}}| \times \int_0^\infty dp |\phi_p(z)\rangle \langle \phi_p(z)|. \quad (3)$$

The potential $V(\mathbf{R}, z)$ being periodic in \mathbf{R} , the solution of (1) can be decomposed into a sum of diffracted waves extended over all the reciprocal surface lattice vectors \mathbf{G} :

$$|\psi_i^+\rangle = \sum_{\mathbf{G}} \psi_{\mathbf{G}}(z) \exp[i(\mathbf{K}_i + \mathbf{G}) \cdot \mathbf{R}] \quad (4)$$

where the subscript i refers to the incident condition. $\psi_{\mathbf{G}}(z)$ is expanded into the continuous set $\phi_p(z)$, that is to say

$$\psi_{\mathbf{G}}(z) = \int_0^\infty b_{\mathbf{G}}(p) \phi_p(z) dp. \quad (5)$$

Now in the right hand side of (1) the Green operator is multiplied on the left by the projector (3), $|\psi_i^+\rangle$ is replaced by the expansion (4) taking account of (5), and the potential $V(\mathbf{R}, z)$ is expanded into Fourier components :

$$V(\mathbf{R}, z) = \sum_{\mathbf{G}} v_{\mathbf{G}}(z) \exp(i\mathbf{G} \cdot \mathbf{R}) \quad (6)$$

with

$$v_{\mathbf{G}}(z) = \frac{1}{S} \int_{\text{u.c.}} V(\mathbf{R}, z) \exp(-i\mathbf{G} \cdot \mathbf{R}) d\mathbf{R} \quad (7)$$

where S is the area of the unit cell (u.c.). A straightforward calculation gives an expression of $|\psi_i^+\rangle$ which is identified with the expansion (4). One obtains the wave function of each channel :

$$|\psi_{\mathbf{J}}(z)\rangle = |\phi_{p_i}(z)\rangle \delta_{\mathbf{J}\mathbf{0}} + \frac{1}{B^2} \sum_{\mathbf{G}} \int_0^\infty dq b_{\mathbf{G}}(q) \int_0^\infty \frac{E_{\mathbf{J}-\mathbf{G}}(p, q) - \delta_{\mathbf{J}\mathbf{G}} M(p, q)}{e_i - \frac{\hbar^2}{2m} ((\mathbf{K}_i + \mathbf{J})^2 + \alpha^2 p^2) + i\epsilon} |\phi_p(z)\rangle dp \quad (8)$$

$$L_{\mathbf{J}}(r) = \frac{1}{B^2} \left[E_{\mathbf{J}-\mathbf{0}}(r, p_i) - \delta_{\mathbf{J}\mathbf{0}} M(r, p_i) + \sum_{\mathbf{G}} \int_0^\infty dq \frac{(E_{\mathbf{J}-\mathbf{G}}(r, q) - \delta_{\mathbf{J}\mathbf{G}} M(r, q)) L_{\mathbf{G}}(q)}{e_i - \frac{\hbar^2}{2m} [(\mathbf{K}_i + \mathbf{G})^2 + \alpha^2 q^2] + i\epsilon} \right]. \quad (14)$$

The solution of this latter set may be easier to obtain because it does not contain the delta function $\delta(r - p_i)$.

3. Application to the exponential corrugated potential. — For this case the potential is :

$$V(\mathbf{R}, z) = C \exp[-\chi(z - \varphi(\mathbf{R}))]$$

and one takes

$$U(z) = C \exp[-\chi z].$$

3.1 The eigenvalues and eigenvectors of H_0 are very well known [11] as

in which

$$e_p = \frac{\hbar^2}{2m} \alpha^2 p^2 \quad (9)$$

with p a dimensionless variable,

$$E_{\mathbf{J}-\mathbf{G}}(p, q) = \int_{-\infty}^{+\infty} \phi_p^*(z) v_{\mathbf{J}-\mathbf{G}}(z) \phi_q(z) dz \quad (10)$$

$$M(p, q) = \int_{-\infty}^{+\infty} \phi_p^*(z) U(z) \phi_q(z) dz. \quad (11)$$

One finds that equation (8) is the same expression as in the so-called C.C.G.M. theory [10].

The expectation value of (8) with the state $\phi_r(z)$ gives an infinite set of coupled integral equations which determines the unknown dimensionless coefficients $b_{\mathbf{G}}(p)$:

$$b_{\mathbf{J}}(r) = \delta(r - p_i) \delta_{\mathbf{J}\mathbf{0}} + L_{\mathbf{J}}(r) \left[e_i - \frac{\hbar^2}{2m} ((\mathbf{K}_i + \mathbf{J})^2 + \alpha^2 r^2) + i\epsilon \right]^{-1} \quad (12)$$

$$L_{\mathbf{J}}(r) = \frac{1}{B^2} \sum_{\mathbf{G}} \int_0^\infty dq b_{\mathbf{G}}(q) \times \left[E_{\mathbf{J}-\mathbf{G}}(r, q) - \delta_{\mathbf{J}\mathbf{G}} M(r, q) \right]. \quad (13)$$

Apart from a normalization factor $L_{\mathbf{J}}(r)$ is equal to the t matrix element

$$t_{\mathbf{J},i} = \langle e^{i(\mathbf{K}_i + \mathbf{J}) \cdot \mathbf{R}} \phi_r(z) | V(\mathbf{R}, z) - U(z) | \psi_i^+ \rangle.$$

The set of integral equations between these elements is readily obtained by replacing in (13) the $b_{\mathbf{G}}(q)$ by their expression (12). One gets :

$$e_p = \frac{(\hbar\chi)^2}{8m} p^2, \quad (15)$$

$$p = \frac{2k_z}{\chi} \quad \text{and from (9)} \quad \alpha = \frac{\chi}{2}$$

$$e^{i\mathbf{K} \cdot \mathbf{R}} \phi_p(z) = \left(\frac{p \sinh(\pi p)}{\pi} \right)^{1/2} K_{ip}(y) e^{i\mathbf{K} \cdot \mathbf{R}} \quad (16)$$

$$y = \frac{(8mC)^{1/2}}{\chi\hbar} \exp\left(-\frac{\chi z}{2}\right) \quad (17)$$

where K_{ip} is the modified Bessel function of the second kind of imaginary order ip . Its integral repre-

sentation [12] shows immediately that this function has only real values and that it tends to zero as z tends to $-\infty$. The asymptotic expansion allows us to determine its limiting value as z tends to $+\infty$, which gives :

$$z \rightarrow +\infty, \quad \phi_p(z) \rightarrow \sin\left(\frac{\chi}{2}pz - \beta_p\right) \quad (18)$$

$$\beta_p = \arg\left[\left(\frac{2mC}{\chi^2\hbar^2}\right)^{ip/2} (\Gamma(1+ip))^{-1}\right]. \quad (19)$$

In this limit, for a given eigenvalue, the constant C yields only a modification of the phase shift.

In order to determine the normalization factor B^2 one considers the potential $U(z)$ limited by an infinite wall at $z = l$ with l positive and very large. In the vicinity of the wall the eigenfunctions are given by (18). They should vanish for $z = l$ and this gives the discrete set of values p_n taken by the parameter p

$$\frac{\chi}{2}p_n l - \beta_{p_n} = n\pi.$$

The normalization integral over the interval $-\infty, l$ can be solved [13] and the result shows that when l increases indefinitely it behaves like

$$\langle \phi_{p_m} | \phi_{p_n} \rangle \begin{cases} 0 & \text{if } p_m \neq p_n \\ = \frac{l}{2} & \text{if } p_m = p_n. \end{cases}$$

Omitting the component due to \mathbf{R} variable, the projector is given by

$$\frac{2}{l} \sum_{n=0}^{\infty} |\phi_{p_n}\rangle \langle \phi_{p_n}|. \quad (20)$$

Now taking the limit $l \rightarrow +\infty$ of (20) and comparing the result to expression (3) one gets

$$B^2 = \frac{\pi}{\chi}. \quad (21)$$

The Fourier components of the potential are proportional to $U(z)$:

$$v_{\mathbf{G}}(z) = v_{\mathbf{G}} U(z),$$

$$\psi_{\mathbf{J}}(z) = \phi_{p_{\mathbf{J}}}(z) \delta_{\mathbf{J}\mathbf{0}} - \frac{\pi^2}{4} I_{-ip_{\mathbf{J}}}(y) \sum_{\mathbf{G}} (v_{\mathbf{J}-\mathbf{G}} - \delta_{\mathbf{J}\mathbf{G}}) \int_0^{\infty} dq b_{\mathbf{G}}(q) \left(\frac{q \sinh(\pi q)}{\pi}\right)^{1/2} \frac{(p_{\mathbf{J}}^2 - q^2)}{\cosh(\pi p_{\mathbf{J}}) - \cosh(\pi q)} +$$

+ terms proportional to $\exp(-\chi z)$

where

$$I_{-ip_{\mathbf{J}}}(y) = \exp[i(p_{\mathbf{J}}\chi z/2 + \beta_0)] \sum_{m=0}^{\infty} \frac{\exp - m(\chi z + 2\beta_0(p_{\mathbf{J}})^{-1})}{m! \Gamma(m+1 - ip_{\mathbf{J}})}$$

with

$$\beta_0 = \arg\left[\left(\frac{(8mC)^{1/2}}{2\chi\hbar}\right)^{-ip_{\mathbf{J}}}\right]$$

$$v_{\mathbf{G}} = \frac{1}{S} \int_{\text{u.c.}} \exp[-i\mathbf{G}\cdot\mathbf{R} + \chi\phi(\mathbf{R})] d\mathbf{R}. \quad (22)$$

If the amplitude of the corrugation function is written as ha , where a is a typical length of the surface lattice and h a dimensionless parameter, the constant $v_{\mathbf{G}}$ depend upon the product χha . Particularly they increase with χ to reach infinite value for the HCWP.

From expression (10) one sees immediately that

$$E_{\mathbf{J}-\mathbf{G}}(p, q) = v_{\mathbf{J}-\mathbf{G}} M(p, q)$$

the matrix element M being equal to [11]

$$M(p, q) = \frac{\pi\chi\hbar^2}{16m} f(p, q)$$

with

$$\begin{cases} p \neq q; f(p, q) = [p \sinh(\pi p) q \sinh(\pi q)]^{1/2} \times \\ \quad \times \frac{(p^2 - q^2)}{\cosh(\pi p) - \cosh(\pi q)} \\ p = q; f(p, q) = \frac{2}{\pi} p^2. \end{cases} \quad (23)$$

3.2 With the above quantities, the wave function of each beam is given by expression (8), which appears as :

$$\psi_{\mathbf{J}}(z) = \phi_{p_{\mathbf{J}}}(z) \delta_{\mathbf{J}\mathbf{0}} + \frac{1}{2} \sum_{\mathbf{G}} (v_{\mathbf{J}-\mathbf{G}} - \delta_{\mathbf{J}\mathbf{G}}) \times$$

$$\times \int_0^{\infty} dq b_{\mathbf{G}}(q) \int_0^{\infty} \frac{f(p, q) \phi_p(z)}{p_{\mathbf{J}}^2 - p^2 + i\varepsilon} dp \quad (24)$$

in which

$$p_{\mathbf{J}}^2 = \frac{4}{\chi^2} [|\mathbf{k}_{\mathbf{J}}|^2 - (\mathbf{K}_{\mathbf{J}} + \mathbf{J})^2] = \frac{4}{\chi^2} (k_{\mathbf{Jz}})^2.$$

Upon carrying out the second integral in (24) the limit of each $\psi_{\mathbf{J}}(z)$ is found to be zero as $z \rightarrow -\infty$. An expression suitable for looking at the limit $z \rightarrow +\infty$ is found in Appendix 1 and appears as :

— for an open channel ($p_{\mathbf{J}}^2 > 0$)

— for a closed channel ($p_J^2 < 0$) : the wave function is given by the same expression as above replacing p_J by $i|p_J|$. Note that in this case δ_{J0} is always equal to zero.

Each of these wave function is a sum of one plane wave and many exponentially damped waves for the case of an open channel. For a closed channel the plane wave is transformed into an exponentially damped one.

Taking the limit $z \rightarrow +\infty$ one finds $\psi_J(z) = 0$ for $p_J^2 < 0$, and for $p_J^2 > 0$

$$\begin{aligned} \psi_J(z) &= \delta_{J0} \sin(k_{iz} z - \beta_{p_i}) + \\ &\quad + A_J \exp i(k_{Jz} z - \beta_{p_J}) \\ A_J &= -\frac{\pi}{4} (p_J)^{-1} \sum_{\mathbf{G}} (v_{J-\mathbf{G}} - \delta_{J\mathbf{G}}) \times \\ &\quad \times \int_0^\infty dq b_{\mathbf{G}}(q) f(p_J, q) \end{aligned} \tag{25}$$

where β_p and $f(p, q)$ are given respectively by (19) and (23). The constant C enters only into the phase shift β_{p_J} , as a variation of C produces a translation of the potential. The wave amplitude A_J may be seen as a sum of contributions given by each open or closed channel, each of them being proportional to the Fourier coefficient of the potential which links the two channels \mathbf{J} and \mathbf{G} .

Therefore the reflection coefficients of the diffracted waves are given by

$$\begin{aligned} R_{J=0} &= |1 + 2iA_0|^2, \\ R_J &= k_{Jz}(k_{iz})^{-1} |2A_J|^2. \end{aligned} \tag{26}$$

3.3 It remains to write the integral equations which allow the determination of the coefficients $b_{\mathbf{G}}(q)$. The set of $L_J(r)$ is given by (14). Putting

$$F_J(r) = \frac{16m}{\chi^2 \hbar^2} L_J(r)$$

one gets

$$\begin{aligned} F_J(r) &= (v_{J0} - \delta_{J0}) f(r, p_i) + \\ &\quad + \frac{1}{2} \sum_{\mathbf{G}} (v_{J-\mathbf{G}} - \delta_{J\mathbf{G}}) \int_0^\infty dq \frac{f(r, q) F_{\mathbf{G}}(q)}{p_{\mathbf{G}}^2 - q^2 + i\epsilon} \end{aligned} \tag{27}$$

with $f(r, q)$ given by (23).

On the other hand from (13) we get a relation between F_J and $b_{\mathbf{G}}$, namely

$$F_J(r) = \sum_{\mathbf{G}} (v_{\mathbf{G}-\mathbf{J}} - \delta_{J\mathbf{G}}) \int_0^\infty dq b_{\mathbf{G}}(q) f(r, q)$$

which compared to (25) gives :

$$A_J = -\frac{\pi}{4} \frac{F_J(p_J)}{p_J} \tag{28}$$

Therefore the solution of the integral equation system (27) allows to calculate directly the wave amplitudes and the reflection coefficients.

4. Numerical solution of the integral equation set. —

Several solutions of the system (27) can be found easily for particular cases or particular values of the variable r . Assume a potential without corrugation, that is to say suppose $\varphi(\mathbf{R}) = 0$. The Fourier coefficients $v_{J-\mathbf{G}} - \delta_{J\mathbf{G}}$ are all equal to zero which implies the solution $F_J(r) \equiv 0, \forall J$. The particles are completely reflected into the specular beam.

Let us consider now an incident angle of 90 degrees. We have $p_i = 0$ and $f(r, p_i) = 0$. The solution $F_J(r) = 0, \forall J$ is a solution of the system and again all the particles are reflected into the 00 beam.

For the variable value $r = 0, f(r, q) = 0$ and we have

$$\forall J, F_J(0) = 0.$$

Note that for the HCWP limit, that is to say for $\chi \rightarrow +\infty$, all the parameters $p_J \rightarrow 0$. The wave amplitude A_J will then be given by the ratio of two numbers going each to zero.

For large values of r the function $f(r, q)$ is proportional to $\exp\left(-\frac{\pi}{2}r\right)$ and $F_J(r)$ will be proportional to the same factor. Consequently the integrand in (27) for large values of q will be proportional to $\exp(-\pi q)$ and the integral is always convergent.

These considerations are all we can say in a general way on the system (27). In order to calculate the diffracted intensities it is now necessary to look for a numerical solution. Whatever the numerical procedure may be, one should keep only a finite number of reciprocal lattice vectors $N_{\mathbf{G}}$, this set including at least all the \mathbf{G} vectors corresponding to the open channels. Also one should limit the integration over the q variable within the interval $[0, q_M]$, q_M being much greater than the largest value of the $p_{\mathbf{G}}$ numbers ($p_{\mathbf{G}}^2 > 0$).

The procedure adopted in the previous work [8] consist in dividing the segment $[0, q_M]$ into N equal intervals $\Omega = q_M(N)^{-1}$ and replacing the continuous function $F_J(r)$ by the discrete set

$$F_{Jn} = \int_{n\Omega}^{(n+1)\Omega} F_J(r) dr.$$

In this way a matrix equation is obtained, the size of the matrix to be inverted being equal to $N_{\mathbf{G}} \times N$. In order to get a solution which gives an unitarity value close to one it is necessary to increase the matrix size as the Fourier coefficients increase with the dimensionless product χha . We were in this way limited in the calculation to χha value less than 0.1, with the integral equation set for the $b_{\mathbf{G}}(q)$ coefficients given by expression (12). This limitation will likely appear for approximately the same χha value

with the new integral equation set of this paper, and one must look for another procedure.

Another way is to expand the $F_{\mathbf{G}}(q)$ into an infinite set of Laguerre polynomials. Again keeping $N_{\mathbf{G}}$ reciprocal lattice vectors and N_L Laguerre coefficients one has a matrix of size $N_{\mathbf{G}} \times N_L$ to be inverted. The same limitation as before appears and this procedure does not seem to be convenient.

Thus the idea of trying an iterative process arises. The obvious starting point is to write $F_{\mathbf{G}}(r) \equiv 0$ corresponding to either an incident angle of 90 degrees or to a flat corrugation $\varphi(\mathbf{R}) = 0$. The second iteration gives

$$F_{\mathbf{G}}^{(1)}(r) = (v_{\mathbf{G}\mathbf{O}} - \delta_{\mathbf{G}\mathbf{O}}) f(r, p_i)$$

which is the starting point of the well known Neumann iteration process in the theory of integral equations. Generally speaking this process is well known to converge to the right solution $F_{\mathbf{G}}(r)$ for small values of the relevant parameter. In our case, the kernel is proportional to the Fourier coefficients $(v_{\mathbf{J}-\mathbf{G}} - \delta_{\mathbf{J}\mathbf{G}})$. Then the convergence criterion for a system of integral equations solved by Neumann iteration [14] shows that the procedure diverges for values of χha larger than say $(\chi ha)_a$. The determination of this value in an analytic way seems to be intractable. Thus the convergence (or divergence) of the solution obtained will be appreciated by comparing to unity the sum of all the diffracted beam reflection coefficients, called the unitarity in the following paragraphs. Note that $(\chi ha)_a$ depends on the surface cell and on the corrugation function shape. Also note that the $p_{\mathbf{G}}$ numbers are inversely proportional to χ hence the $(\chi ha)_a$ value obtained could be different depending on whether χ or h vary independently, all other quantities being constant.

For purposes of numerical calculation the way by which the integral in the right hand side of (27) can be handled is given in Appendix 2.

5. Convergence-divergence. — Let us consider now and in the subsequent paragraphs a particle of wave vector $|\mathbf{k}_i| = 8.6 \text{ \AA}^{-1}$ which is scattered by a periodic lattice with a square unit cell (parameter

$a = 2.55 \text{ \AA}$). The incident plane contains the [100] direction ($\varphi = 45^\circ$). The corrugation function is taken as

$$\varphi(\mathbf{R}) = ha \left[\cos\left(\frac{2\pi x}{a}\right) + \cos\left(\frac{2\pi y}{a}\right) \right]$$

and the Fourier components $v_{\mathbf{G}}$ are equal to

$$v_{\mathbf{G}} = I_{G_x}(\chi ha) I_{G_y}(\chi ha), \quad \mathbf{G} = G_x \mathbf{O}_x + G_y \mathbf{O}_y$$

with I the modified Bessel function of the first kind.

These conditions correspond to an experiment in which a molecular hydrogen beam produced by a nozzle source at room temperature is scattered by a copper (100) face.

In order to study the convergence of the iterative process we choose an incident angle of 31 degrees (with respect to the surface normal). There are 37 open channels. The χ and h parameter values will vary independently.

Figure 1 gives the evolution of the unitarity calculated at each iteration step $U^{(n)}$ versus the iteration number n , for different values of the potential damping coefficient χ , with $h = 0.02$. Table I gives the $U^{(n)}$ value for $n = 5, 10, 15, 20, 25$.

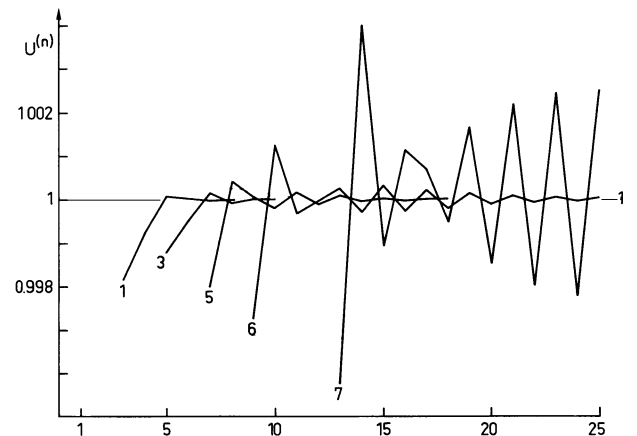


Fig. 1. — Evolution of the unitarity calculated at each iteration step $U^{(n)}$ with the number of iterations. Each curve is labelled by a number which is the value of χ in \AA^{-1} , $|\mathbf{k}_i| = 8.6 \text{ \AA}^{-1}$, $\theta_i = 31^\circ$, $\varphi = 45^\circ$, and $h = 0.02$.

Table I. — Evolution of the unitarity $U^{(n)}$ as a function of the number of iteration n for different values of χ . $N_{\mathbf{G}}$ is the number of reciprocal lattice vectors introduced into the numerical calculation, $|\mathbf{k}_i| = 6.8 \text{ \AA}^{-1}$, $a = 2.55 \text{ \AA}$, $h = 0.02$, and $\theta_i = 31^\circ$.

$\chi \text{ \AA}^{-1}$	1	3	5	6	7	8
χha	0.051	0.153	0.255	0.306	0.357	0.408
$N_{\mathbf{G}}$	81	81	81	109	121	121
$U^{(1)}$	1.103 313 47	1.370 412 78	1.489 894 82	1.531 459 27	1.570 065 96	1.608 969 23
$U^{(5)}$	1.000 066 85	0.998 797 31	0.987 866 12	0.976 649 31	0.965 153 30	0.972 503 34
$U^{(10)}$	0.999 999 99	0.999 997 43	0.999 814 46	1.001 258 58	1.017 704 41	1.149 669 95
$U^{(15)}$		0.999 999 96	1.000 027 67	1.000 295 97	0.998 904 91	1.017 866 59
$U^{(20)}$		0.999 999 98	0.999 998 07	0.999 886 08	0.998 547 01	1.336 965 22
$U^{(25)}$				1.000 030 94	1.002 462 67	

A quick inspection of these data shows immediately that for $\chi \leq 6 \text{ \AA}^{-1}$ the $U^{(n)}$ values are successively greater and lower than unity and that the unitarity defect $\Delta^{(n)} = |U^{(n)} - 1|$ decreases continuously with n , provided a sufficiently large value of n is considered. For a given χ value, if the number of reciprocal lattice vectors introduced into the numerical calculation is increased the $\Delta^{(n)}$ becomes smaller, provided the initial value of n is sufficiently large. These facts characterize a convergent process.

For $\chi = 7 \text{ \AA}^{-1}$ the iteration seems to converge until a value $n = 18$ but beyond this value $\Delta^{(n)}$ increases slowly but continuously. The iteration leads to a divergent solution. Nevertheless it is interesting to look at the behaviour of the different calculated reflection coefficients $R_{G_x, G_y}^{(n)}$. Some of them behave like $U^{(n)}$ respectively for $\chi = 6 \text{ \AA}^{-1}$ (convergent) and for $\chi = 7 \text{ \AA}^{-1}$ (divergent). For others the $R^{(n)}$ value decreases continuously with n ; this is mainly the case for high index beams ($\overline{23}$, $\overline{33}$, $\overline{34}$...) for which $R^{(n)}$ is very low, say less than 10^{-5} .

Table II. — Evolution of the unitarity $U^{(n)}$ as a function of the number of iterations n for different values of h . N_G is the number of reciprocal lattice vectors introduced into the numerical calculation, $|\mathbf{k}_i| = 6.8 \text{ \AA}^{-1}$, $a = 2.55 \text{ \AA}$, $\chi = 3 \text{ \AA}^{-1}$, and $\theta_i = 31^\circ$.

h	0.02	0.04	0.045	0.05
χha	0.153	0.306	0.344 25	0.382 5
N_G	100	100	121	121
$U^{(1)}$	1.370 412 78	2.628 974 45	3.130 167 86	3.726 279 22
$U^{(5)}$	0.998 797 47	1.479 210 82	3.249 934 92	10.722 045 43
$U^{(10)}$	0.999 997 43	1.053 590 34	1.783 780 44	13.749 577 1
$U^{(15)}$	0.999 999 96	0.992 138 41	1.055 782 03	
$U^{(20)}$	0.999 999 98	0.998 760 30	0.985 245 74	
$U^{(25)}$			1.052 382 85	

Table III. — Reflection coefficients of the most significant beams as a function of χ . HCWP correspond to an infinite value of χ . E_z is the normal kinetic energy ratio of the beam considered to that of the specular,

$$|\mathbf{k}_i| = 6.8 \text{ \AA}^{-1}, \quad a = 2.55 \text{ \AA}, \quad h = 0.02, \quad \text{and} \quad \theta_i = 31^\circ.$$

$\chi \text{ \AA}^{-1}$	1	3	5	6	7	HCWP	E_z
R_{00}	0.903 7	0.695 8	0.629 4	0.614 5	0.605 1	0.583 0	1
$R_{11} \times 100$	0.16×10^{-6}	0.038 16	0.187 8	0.253 6	0.305 3	0.498 7	0.208
$R_{10} \times 10$	0.37×10^{-2}	0.367 1	0.618 8	0.678 5		0.822 6	0.604
$R_{\overline{11}} \times 10$	0.41×10^{-3}	0.049 2	0.088 3	0.098 0	0.104 2	0.126 8	0.776
$R_{0\overline{1}}$	0.043 2	0.096 7	0.098 7	0.098 73		0.100 5	1.17
$R_{\overline{1}\overline{1}} \times 10$	0.027 6	0.163 0	0.185 9	0.189 7	0.191 8	0.208 4	1.34

Table IV. — Same as table III for $\theta_i = 60.5^\circ$.

$\chi \text{ \AA}^{-1}$	1	3	5	6	7	HCWP	E_z
R_{00}	0.999 8	0.959 5	0.916 9	0.905 1	0.897 0	0.872 9	1
$R_{0\overline{1}} \times 10$	0.58×10^{-3}	0.190 4	0.382 0	0.434 0	0.469 2	0.573 4	2.11
$R_{\overline{1}\overline{1}} \times 100$	0.63×10^{-5}	0.110 3	0.357 0	0.442 8	0.504 9	0.741 3	3.23
$R_{1\overline{1}} \times 10^3$	0.31×10^{-4}	0.088 9	0.364 9	0.486 4	0.581 6	0.773 4	0.322

For $\chi = 8 \text{ \AA}^{-1}$ the $U^{(n)}$ and the different $R^{(n)}$ values increase with n and the numerical iterative process does not converge.

Table II gives the same quantities as above when h varies with $\chi = 3 \text{ \AA}^{-1}$. The process is convergent for $h \leq 0.04$ and is divergent above this value. For $h = 0.045$ the $U^{(n)}$ and $R^{(n)}$ behaviour is identical to that described above for $\chi = 7 \text{ \AA}^{-1}$.

Therefore the two variables χ and h are symmetric with respect to the convergence criterion in spite of the fact that the p_j number are inversely proportional to χ and independent of h . The Neumann iterative process yields a convergent solution for χha less than or equal to 0.34 for the particular system depicted at the beginning of this paragraph.

6. Results. — 6.1 Tables III and IV give the calculated reflection coefficients for increasing value of χ with $h = 0.02$ for incident angles of 31 and 60.5 degrees respectively. The most significant values only are given, the others being at least two orders of magnitude smaller. Of course, the calculated results reflect the symmetry of the chosen incident conditions, i.e. one always finds $R_{G_x, G_y} = R_{G_y, G_x}$. For the HCWP the R values have been calculated using the Fourier expansion of the source function [15] and a new method for carrying out the resulting integrals [16].

The following facts can be readily observed :

- as expected, when χ increases, the HCWP solution is approached ;
- the intensity in the specular beam is greater than the limit given by the HCWP. The inverse behaviour is displayed by all the other diffracted beams ;
- all the beam intensities vary rapidly for low χ value, more precisely, for χ less than 3 \AA^{-1} . Beyond this value the variation is smoother ;

— among the diffracted beams ($G \neq 0$), at least for the incident angle of 31 degrees, the relative difference between intensities given by the ECP and HCWP is small for the peaks 01, $1\bar{1}$ and large for the other three. It can be noticed that these two groups are composed of subspecular and supraspecular beams respectively.

6.2 Let us suppose now that the incident angle θ_i decreases in the vicinity of θ_M , the incident angle for which the beam labelled by the reciprocal vector \mathbf{M} is emerging. The corresponding value of p_M^2 which is negative passes through zero and becomes positive. In the sum over reciprocal lattice vectors of equation (27) this produces the appearance of a delta function $\delta(p_M^2 - q^2)$ as soon as p_M^2 becomes positive. Therefore one can expect to observe on the reflection coefficient of each open beam a disturbance at $\theta_i = \theta_M$. Furthermore this disturbance should be most important for the diffracted peak \mathbf{J} having the largest Fourier coefficient $v_{\mathbf{J}-\mathbf{M}} - \delta_{\mathbf{J}\mathbf{M}}$, i.e. for beams \mathbf{J} strongly coupled with the emerging one. Consequently this effect will be important for the emerging beam itself and for those having a \mathbf{J} vector close to \mathbf{M} . Also its importance will increase with the product χha and particularly will be maximum in the case of HCWP.

Following these qualitative considerations it is interesting to study the case where the most intense and the emerging beams are strongly coupled. With the system adopted for numerical calculation, this happens when the 10 and 01 beams emerge, i.e. for an incident angle $\theta_M = 50.96$ degrees. Figure 2 gives the Ewald diagram for this condition.

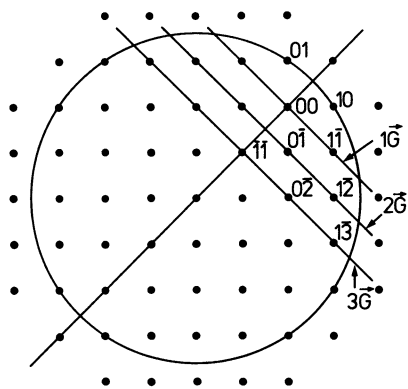


Fig. 2. — Ewald diagram for $\theta_i = 50.96^\circ$. The 10 and 01 beams are emerging $|k_i| = 8.6 \text{ \AA}^{-1}$ and we have taken a square lattice of parameter $a = 2.55 \text{ \AA}$. The lines connect the points representing the open channels coupled to the 10 beam by the first, second, and third shortest reciprocal lattice vectors.

As far as the 01 (10) beam is concerned the calculation with the ECP indicates that the derivative of the reflection coefficient with respect to incident angle for $\theta_i = \theta_M$ is infinite as in the HCWP case [1]. However

the corresponding intensity being very small, strictly equal to zero for $\theta_i = \theta_M$, its variation is not experimentally detectable.

Figure 3 gives the evolution of the reflection coefficient for the 00 and $1\bar{1}$ beams, the two beams coupled to the 10 by one of the smallest reciprocal lattice vectors. In the case of HCWP, in agreement with previous results [1], one observes a discontinuity on the slope $dR/d\theta_i$ for $\theta_i = \theta_M$, the slope being infinite just when the 10 and 01 beams are emerging. With the ECP this kind of singularity persists but tends to disappear as χ decreases. However, the slope on the emerging beam side always has a finite value.

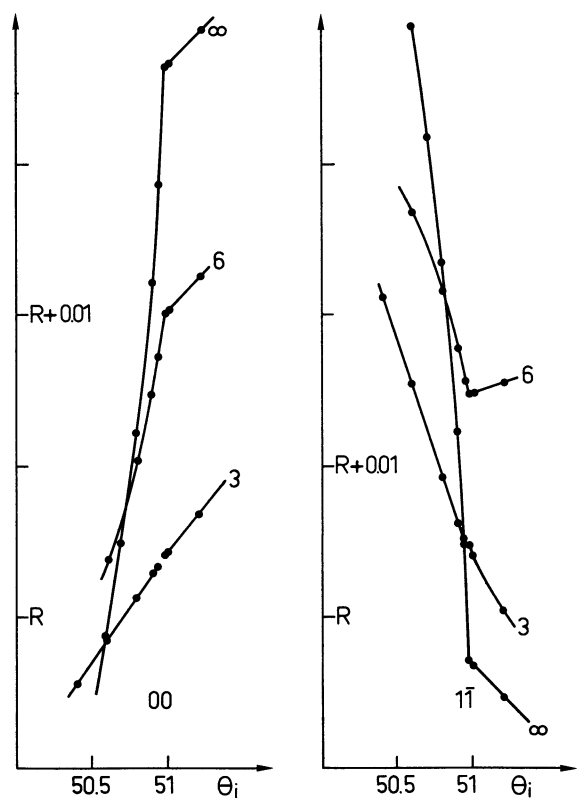


Fig. 3. — Evolution of the reflection coefficient for the 00 and $1\bar{1}$ beams in the vicinity of $\theta_i = 50.96$ where the 10 and 01 beams are emerging. The number which labels each curve gives the value of χ ($\chi \rightarrow \infty \Rightarrow$ HCWP). For $\chi = 3 \text{ \AA}^{-1}$, $R_{00} = 0.905$, and $R_{1\bar{1}} = 0.33$. For $\chi = 6 \text{ \AA}^{-1}$, $R_{00} = 0.84$ and $R_{1\bar{1}} = 0.08$. For $\chi \rightarrow \infty$ $R_{00} = 0.805$, $R_{1\bar{1}} = 0.16$. $R_{1\bar{1}}$ is multiplied by $10^3 (3 \text{ \AA}^{-1})$ and by 10^2 for the other χ values.

Figure 4 gives the same evolution as above for the $0\bar{1}$ and $1\bar{1}$ beams which are respectively coupled to the 10 by the second and third smallest reciprocal lattice vectors. Here the singularity at θ_M is of different shape resembling rather a singularity given by a resonance with bound state. It disappears as χ decreases, more rapidly than in the preceding case.

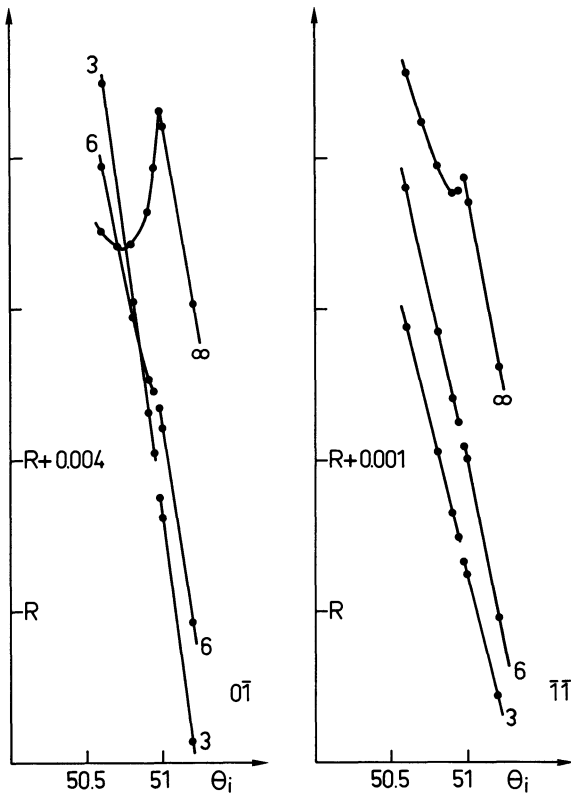


Fig. 4. — Evolution of the reflection coefficient for the 0I and II beams in the vicinity of $\theta_i = 50.96$ where the 10 and 01 beams are emerging. The number which labels each curve gives the value of χ (with $\chi \rightarrow \infty \Rightarrow$ HCWP). For $\chi = 3 \text{ \AA}^{-1}$, $R_{0\bar{1}} = 0.424$, and $R_{\bar{1}\bar{1}} = 0.037$. For $\chi = 6 \text{ \AA}^{-1}$, $R_{0\bar{1}} = 0.664$ and $R_{\bar{1}\bar{1}} = 0.085$. For $\chi \rightarrow \infty$ $R_{0\bar{1}} = 0.773$ and $R_{\bar{1}\bar{1}} = 0.117$. All the R values are multiplied by 10.

7. Discussion. — Following the above result (see expression (25)) each open or closed channel gives a contribution to the wave amplitude of a diffracted beam. The equation giving the wave amplitude contains a sum over all the reciprocal lattice vectors. This is clearly an effect of multiple scattering.

As a consequence the set of integral equations (27), which allows the calculation of wave amplitudes and reflection coefficients, as well as the equation which determines the source function for the HCWP case, contains a similar sum.

In each case the infinite sum is truncated for purpose of numerical solution and a finite number of reciprocal lattice vectors, and correspondingly of potential Fourier components N_G , is retained. In this situation one verifies that the calculated unitarity U_{N_G} is never equal to one but the unitarity defect $|U_{N_G} - 1|$ becomes smaller and smaller when N_G increases, provided the numerical procedure used leads to a convergent solution. Therefore the solution obtained is close to the exact result which would be obtained in the limit $N_G \rightarrow \infty$. The gap between them, corresponding to the neglected G vector contributions, may be characterized by the value of the unitarity defect

which in turn gives, roughly speaking, the maximum error on the calculated reflection coefficient values. In particular the values which are less than the unitarity defect may not be significant. Fortunately with the modern computer available one can introduce into the numerical calculation a large number of reciprocal lattice vectors such that the unitarity defect should be less than the sensitivity of experimental measurement. Thus we are sure to obtain a solution with a potential containing all its Fourier components with sufficient precision.

Taking the HCWP results as a reference one sees at first sight that the overall effect of the ECP is to enhance the specular intensity and to reduce all the others. As these intensity modifications become more and more important when the potential damping coefficient χ decreases they should be ascribed to the effect of the increasing wave penetration into the potential region. In order to clarify this point let us recall first that each diffraction channel is described by the product of two wave functions, $\psi_j(z) \exp[i(\mathbf{K}_i + \mathbf{J}) \cdot \mathbf{R}]$. Obviously the wave penetration affects only the normal component $\psi_j(z)$, to which corresponds a normal kinetic energy E_{jz} proportional to p_j^2 . For this energy the potential slope is given by

$$\left(\frac{dV}{dz}\right)_{V=E_{jz}} = -\chi E_{jz}.$$

Therefore as far as the wave penetration is concerned, each wave $\psi_j(z)$ feels a potential region in which the potential slope is different. The higher the absolute value of the slope, or equivalently the higher the normal kinetic energy, the lower is the wave penetration.

Let us now consider the 10 and 0I beams (Table III) for which the multiple scattering effect is certainly equivalent as each of them is linked to the 00 beam by one of the smallest reciprocal lattice vectors. Considering the relative E_z value (see Table III) the wave penetration is lower for the 0I beam than for the 10. The intensity reduction of each beam, taking the HCWP result as reference, is also proportionally lower for the former confirming that to a lower wave penetration corresponds a lower intensity reduction. The same analysis can be done for the group composed of the 11, 1I and II beams. If these beams are classed by order of increasing wave penetration i.e. II, 1I and 11, we obtain the order of increasing intensity modification.

For the incident angle of 60.5 degrees (Table IV) the comparison can be done only with the pair 1I and II. Following the preceding analysis the intensity reduction should be greater for the 1I than for the II but the results show that they are approximately equivalent. It should be noticed however that their nearest neighbour beams are very much different.

The 1I has two closed and two open channels whereas the II has four open channels. Thus the

multiple scattering effect is different for either beam and it seems that the proximity of closed channels enhances the intensity.

The results concerning the disturbance appearing when a beam is emerging are in agreement with the qualitative behaviour deduced from the integral equations (27). The disturbance is greatest for beams strongly coupled with the emerging one, i.e. linked together by small reciprocal lattice vectors, and becomes more important as χ increases. The shape of the disturbance reflects the fact that the coupling involves one or many reciprocal lattice vectors. We propose to call these perturbations of the intensity variation emerging beam singularities of the first and second type, respectively. The second type seems to be like a perturbation due to a bound state resonance. Such a shape is expected since an emerging beam is precisely at the threshold resonance condition. The practical interest of merging singularities should be outlined. As their shape seems to be very sensitive to the χ value, this seems to be a good way to obtain an approximate value of χ if one has a set of reliable experimental data. Experimentalists are urged to make such measurements.

One might ask if the behaviour of the scattering pattern given by the ECP and analysed in one particular case here can be considered as general. For instance one can wonder if with a greater h value, in a region where the rainbow pattern appears, the same beam intensity modifications or the same emerging beam singularities happen. It is always hasardous to answer such a question. However as our present results have been qualitatively explained on the basis of some simple physical ideas one can infer that the whole qualitative behaviour will occur. In particular it is likely that the effect of wave penetration as discussed above, will certainly play an important role and

perhaps yield a modification of the beam intensities which will be more important for a greater h value, the multiple scattering being then more important. In the same way it is likely that the emerging beam singularities will be visible as their appearance can be predicted from the form of the integral equations.

8. Conclusion. — The scattering of neutral atoms by an exponential corrugated potential has been solved exactly. Compared to our previous work [8] the solution has been extended to real bidimensional corrugated surfaces and the infinite set of integral equations involving t matrix elements which are directly linked to the beam wave amplitude has been solved numerically. The convergence domain is extended from $\chi ha = 0.1$ to $\chi ha = 0.34$. Now we are able to obtain numerical results up to medium amplitude surface corrugations.

Compared to the results given by the well known hard corrugated wall potential, the exponential corrugated potential yields an enhancement of the specular intensity and a reduction of all the others. It modifies also the shape and importance of the singularities which appear on beam intensities when one or more beams are simultaneously emerging.

This latter effect can be predicted on the basis of the integral equation form. As the integral equations written in the general case (expression (14)) always have the same structure these singularities should happen whatever the potential may be.

Acknowledgments. — It is a pleasure to thank Dr C. Manus for his constant encouragement, Drs D. A. Degras and J. Lapujoulade for stimulating discussions, and particularly Prof. J. R. Manson from Clemson University with whom this work was initiated during his stay in Saclay.

Appendix 1

The last integral of formula (24) can be written as :

$$\left(\frac{q \sinh(\pi q)}{\pi}\right)^{1/2} \int_0^{\infty} \frac{g(p, q)}{(p^2 - p^2 + i\epsilon)} p K_{ip}(y) dp, \quad g(p, q) = \frac{\sinh(\pi p)(p^2 - q^2)}{\cosh(\pi p) - \cosh(\pi q)}$$

$K_{ip}(y)$ and $pg(p, q)$ are even functions with respect to the p variable. Therefore the integration can be taken from $-\infty$ to $+\infty$.

From the recurrence relation between the K functions one deduces easily that

$$p K_{ip} = \frac{y^2}{4i(1+p^2)} [K_{ip+2} - K_{ip-2} + ip(2K_{ip} - K_{ip+2} - K_{ip-2})].$$

The integral now becomes

$$W = \frac{y^2}{8i} \sum_{n=1}^3 \int_{-\infty}^{+\infty} \frac{g(p, q)}{(p^2 - p^2 + i\epsilon)} \frac{1}{(1+p)^2} D_n(p) dp$$

where, upon using the integral representation of K function [12],

$$D_1 = \int_{-\infty}^{+\infty} \sinh (2 \alpha) \exp(ip\alpha - y \cosh (\alpha)) d\alpha ,$$

$$D_2 = ip \int_{-\infty}^{+\infty} \exp(ip\alpha - y \cosh (\alpha)) d\alpha ,$$

and

$$D_3 = - ip \int_{-\infty}^{+\infty} \cosh (2 \alpha) \exp(ip\alpha - y \cosh (\alpha)) d\alpha .$$

This gives

$$W = \frac{y^2}{8} \int_{-\infty}^{+\infty} d\alpha \exp(-y \cosh (\alpha)) [(1 - \cosh (2 \alpha)) w_1 - i \sinh (2 \alpha) w_0]$$

with

$$w_m = \int_{-\infty}^{+\infty} \frac{g(p, q)}{(p_J^2 - p^2 + i\varepsilon)} \frac{p^m}{(1 + p^2)} \exp(ip\alpha) dp \quad m = 0, 1 .$$

This last integral is solved in the usual way by taking a contour in the upper half complex plane for $\alpha > 0$, and in the lower half complex plane for $\alpha < 0$. After some lengthy but straightforward calculations one gets :

$$W = g(p_J, q) \left[-\frac{i\pi}{2} K_{ip_J}(y) + \frac{\pi}{4} y^2 \int_0^\infty d\alpha (h_c(y, \alpha) \sin (p_J \alpha) - h_s(y, \alpha) \cos (p_J \alpha) (p_J)^{-1}) \right]$$

$$- 4 y^2 \sum_{n=1}^\infty \Re \left[r_n^{(1)}(p_J, q) \int_0^\infty d\alpha h_c(\alpha, y) \exp(iq - 2n) \alpha \right] + \Im \left[r_n^{(0)}(p_J, q) \int_0^\infty d\alpha h_s(\alpha, y) \exp(iq - 2n) \alpha \right]$$

where

$$h_c(\alpha, y) = (1 - \cosh (2 \alpha)) \exp(-y \cosh (\alpha)) , \quad \text{and} \quad h_s(\alpha, y) = \sinh (2 \alpha) \exp(-y \cosh (\alpha)) .$$

The symbols \Re and \Im mean that one has to take respectively the real and imaginary part of the expression which follows.

The first term comes from the poles of the denominator $p_J^2 - p^2 + i\varepsilon$, and the second from the poles of $g(p, q)$ with the r_n equal their respective residues as follows :

$$r_n^{(m)}(p_J, q) = \frac{n(q + in)}{p_J^2 - (q + i 2 n)^2} \frac{(q + i 2 n)^m}{1 + (q + i 2 n)^2} .$$

This result is valid for $p_J^2 > 0$ (open channel). For $p_J^2 < 0$ (closed channel) W is given by the preceding expression in which p_J is changed into $i |p_J|$. In either case one see immediately that W tends to zero as y goes to infinity or conversely as z goes to minus infinity.

A more interesting expression can be obtained by introducing in the preceding the following relation [12] :

$$\int_0^\infty \exp - (v\alpha + y \cosh (\alpha)) d\alpha = \frac{\pi}{\sin (\pi v)} \left[- I_v(y) + \frac{1}{\pi} \int_0^\pi \cos (v\theta) \exp(y \cos \theta) d\theta \right]$$

in which I is the modified Bessel function of the first kind. One gets :

$$W = g(p_J, q) (\sinh (\pi p_J))^{-1} \left[-\frac{\pi^2}{2} I_{-ip_J}(y) \right.$$

$$\left. + \frac{\pi}{4} y^2 \frac{1}{1 + p_J^2} \int_0^\pi \left(C_c(\theta, y) \cosh (p_J \theta) - C_s(\theta, y) \frac{\sinh (p_J \theta)}{p_J} \right) d\theta \right]$$

$$+ 8 \pi (\sinh (\pi q))^{-1} \sum_{n=1}^{\infty} \begin{cases} \Im[r_n^{(1)}((2n-iq)(2n-1-iq)I_{2n-iq}(y) \\ - yI_{2n+1-iq}(y) + \frac{y^2}{2\pi} \int_0^\pi C_c(\theta, y) \cos((2n-iq)\theta) d\theta)] \\ - \Re[r_n^{(0)}((2n-iq)(2n-1-iq)I_{2n-iq}(y) + y(2n-iq)I_{2n+1-iq}(y) \\ + \frac{y^2}{2\pi} \int_0^\pi C_s(\theta, y) \sin((2n-iq)\theta) d\theta)] \end{cases}$$

with $C_c = (1 - \cos 2\theta) \exp(y \cos \theta)$ and $C_s = \sin(2\theta) \exp(y \cos \theta)$.

Appendix 2

The integral to be calculated numerically at each iteration can be written in the form :

$$In = \int_0^\infty \frac{W_G(r, q)}{p_G^2 - q^2 + i\epsilon} dq.$$

If p_G^2 is negative there is no problem. As $W_G(r, q)$ behaves like $\exp(-\pi q)$ for large q values, integration from 0 to Q with Q very large leads to the neglect of a number of the order or less than $\pi^{-1} \exp(-\pi Q)$.

Let us consider now the case $p_G^2 > 0$.

$$In = -i\pi \frac{W_G(r, p_G)}{2p_G} + P \int_0^\infty \frac{W_G(r, q)}{p_G^2 - q^2} dq$$

where P means the principal value. Looking at the Taylor expansion of W_G , it is easy to show that the function

$$\frac{W_G(r, q) - W_G(r, p_G)}{p_G^2 - q^2}$$

has no singularity for $q = p_G$. Therefore the principal value integral can be rewritten as

$$\int_0^\infty \frac{W_G(r, q) - W_G(r, p_G)}{p_G^2 - q^2} dq + W_G(r, p_G) P \int_0^\infty \frac{dq}{p_G^2 - q^2}$$

or, the last principal value integral being equal to zero,

$$\int_0^Q \frac{W_G(r, q) - W_G(r, p_G)}{p_G^2 - q^2} dq + \int_Q^\infty \frac{W_G(r, q)}{p_G^2 - q^2} dq - W_G(r, p_G) \int_Q^\infty \frac{dq}{p_G^2 - q^2}$$

with Q larger than p_G^2 . For the same reason as above the second integral is less than $\exp(-\pi Q)$ and can be neglected. This gives :

$$In = \left[-i\pi + \text{Log} \left(\frac{Q + p_G}{Q - p_G} \right) \right] \frac{W_G(r, p_G)}{2p_G} + \int_0^Q \frac{W_G(r, q) - W_G(r, p_G)}{p_G^2 - q^2} dq.$$

References

- | | |
|--|---|
| [1] GARCIA, N., <i>J. Chem. Phys.</i> 67 (1977) 897. | [9] WOLKEN, G., <i>J. Chem. Phys.</i> 58 (1973) 3047. |
| [2] LAPUJOLADE, J., LEJAY, Y. and PAPANICOLAOU, N., <i>Surf. Sci.</i> 90 (1979) 133. | [10] CABRERA, N., CELLI, V., GOODMAN, F. O. and MANSON, J. R., <i>Surf. Sci.</i> 19 (1970) 67. |
| [3] GARCIA, N., CELLI, V. and GOODMAN, F. O., <i>Phys. Rev. B</i> 19 (1979) 634. | [11] JACKSON, J. M. and MOTT, N. F., <i>Proc. R. Soc. London, Ser. A</i> 137 (1932) 703. |
| [4] HARVIE, C. E. and WEARE, J. H., <i>Phys. Rev. Lett.</i> 40 (1978) 187. | [12] WATSON, G. N., <i>Theory of Bessel functions</i> (Cambridge University Press) 1962, p. 181. |
| [5] SCHWARTZ, C., COLE, M. W. and PLIVA, J., <i>Surf. Sci.</i> 75 (1978) 1. | [13] GRAY, A. and MATHEWS, G. B., <i>A treatise of Bessel function</i> (Dover New York) 1966, p. 70. |
| [6] KLEIMAN, G. G. and LANDMAN, U., <i>Phys. Rev. B</i> 8 (1973) 5484. | [14] MIKHLIN, S. G., <i>Integral equations</i> (Pergamon press) 1964, p. 31. |
| [7] MANSON, J. R. and ARMAND, G., <i>11th Symp. Rarefied gas dynamics</i> , R. Campagne editor 1979, p. 1373; <i>Phys. Rev. B</i> 20 (1979) 5020. | [15] ARMAND, G. and MANSON, J. R., <i>Phys. Rev. B</i> 18 (1978) 6510. |
| [8] ARMAND, G. and MANSON, J. R., <i>Phys. Rev. Lett.</i> 43 (1979) 1839. | [16] SALANON, B. and ARMAND, G., to be published. |